Propagation Phenomena Affecting Satellite Communication Systems Operating in the Centimeter and Millimeter Wavelength Bands

R. K. CRANE

Abstract—The theories describing the effects of the troposphere on satellite communication systems operating in the microwave region are reviewed. The results of computations based upon the theories and atmospheric models are presented and compared with available experimental data. From the model computations it is seen that rain causes the major propagation problems for the frequency bands allocated to or proposed for allocation to the satellite communications service. Two effects are dominant: attenuation due to rainfall along the line-of-sight and interference between two systems operating at the same frequency and beyond each other's radio horizon due to rain scatter. The methods for calculating the magnitude of the effects of rain given the spatial distribution of rainfall intensity are available. The statistical data required for the prediction of the spatial distribution of rainfall intensity are not available.

Introduction

CENTIMETER wavelength bands are currently being used for satellite communication service and the use of millimeter wave bands is being planned. The imminent use of millimeter wavebands has prompted a number of theoretical and experimental studies of the limitations imposed on line-of-sight, ground-to-space, and space-to-ground communication systems by the atmosphere. The studies have shown that the limitations mainly arise from either signal attenuation or interference by transhorizon propagation phenomena. The principal cause of both attenuation and interference for properly sited terminals is scattering by hydrometeors. At present, the physics of hydrometeor scattering is well understood and, with the exception of scattering by complex bodies such as hail or melting snow, the attenuation and transhorizon scattered field strengths may be computed for a given geometry and distribution of hydrometeors. The statistical description of attenuation or interfering field strengths required for satellite communication systems design is, however, not currently available. This is a consequence of a lack of knowledge of the statistical properties of rain.

This paper reviews the current theories of tropospheric propagation phenomena relevant to satellite communications in the centimeter and millimeter wavelength bands and assesses their relative importance. The approach taken is not to re-derive the theoretical results which are readily available in the literature but to present the results of computations made using the theories or models and to compare the results with available experimental data. The comparisons together with discussions of the possible limitations of the models are used to evaluate their application to the description of tropospheric propagation phenomena. The computations are those of the author, while the experimental results are partially those of the author and partially those of others as referenced.

The effects of the medium on satellite communication systems are evidenced through signal attenuation or slow fading, amplitude scintillation or rapid fading, phase scintillation, receiver noise, and bandwidth limitations. Each of these effects may be due to one or more physical phenomena. A reduction in signal strength may occur due to molecular absorption by atmospheric oxygen and water vapor, attenuation due to rain along the path, focusing loss caused by vertical gradients of refractive index, or antenna gain reduction due to phase decorrelation and wavefront tilt across a large aperture caused by turbulence. In the following sections each of the propagation mechanisms are examined together with their effects. The frequencies of interest are those in the centimeter and millimeter wavelength bands allocated to or planned for allocation to satellite communication services. The lowest frequency of interest is 2 GHz, the highest 148 GHz. The allocations are such that, for frequencies below 10 GHz, the largest bandwidth is 800 MHz and, for frequencies above 10 GHz, the largest bandwidths are 3.5 GHz at 20 and 30 GHz. The frequencies are sufficiently high that, except for possible bandwidth limitations, the effects of the ionosphere may be ignored.

Molecular Absorption

Molecular absorption in the centimeter and millimeter wavelength bands is primarily due to absorption by oxygen and water vapor. Some of the trace gases with polar molecules, such as nitrous oxide, have absorption lines in the millimeter wavelength region but they may be neglected in comparison with oxygen and water vapor. The oxygen molecule has a permanent magnetic moment, and absorption at millimeter wavelengths occurs due to magnetic interaction with the incident field. The interaction produces a family of rotation absorption lines in the vicinity of 60 GHz and an isolated line at 118.8 GHz. Van Vleck and Weisskopf [1] developed a theory for the frequency dependence of the absorption which depends upon an empirical linewidth constant. The linewidth constant is, however, a function of the temperature, pressure, and constit-

Manuscript received September 8, 1970. This work was sponsored by the Department of the Air Force.

The author is with the Lincoln Laboratory, Massachusetts Institute of Technology, Lexington, Mass. 02173.

uents of the gas. Calculations of the attenuation due to oxygen absorption using the Van Vleck, Weisskopf line shape formula and the empirical linewidth constants developed by Meeks and Lilley [2] are in reasonable agreement with measurements as shown by Lenoir, Barrett, and Papa [3]. Additional experimental work near the isolated 118.8-GHz line as reported by Zhevakin and Naumov [4] is in better agreement with the calculations when the linewidth constant for the 118.8-GHz line is increased by 48 percent relative to the other equal linewidth constants. Using the Van Vleck and Weisskopf line shape, the linewidth constants given by Meeks and Lilley for all lines except the one at 118.8 GHz, and a 48-percent larger linewidth constant for the 118.8-GHz line, the zenith attenuation was computed using temperature profile data from the U. S. Standard Atmosphere [5] and is given on the curve labeled 0 percent of Fig 2 shown below.

Water vapor is a polar molecule with an electric dipole which interacts with the incident radiation to produce rotation absorption lines at 22.2 GHz, 183.3 GHz, and higher frequencies. The Van Vleck and Weisskopf line shape together with the empirical linewidth constant derived from the data of Becker and Autler [6] for the 22.2-GHz line by Barrett and Chung [7] and the summation of the contribution of lines at frequencies above 30 GHz as given by Van Vleck [8] have been used to model water vapor absorption. Measurements made by Staelin and by Gaut as reported by Staelin [9] of attenuation at frequencies between 22 and 32 GHz and computations based upon the model and simultaneous radiosonde measurements of the temperature and humidity profiles show agreement to within 5 percent. Measurements made by Zhevakin, Troitsiy, and Tseytlin [10] and others as reported by Zhevakin and Naumov [11] show that the attenuation may be underestimated by a factor of 3 in the 30–150-GHz region when using the above model. They obtained an improvement in the estimate of attenuation in the 30–150-GHz frequency range by using the line shape derived from kinetic theory [12] and linewidths calculated by Benedict and Kaplan [13]. The improved estimate still, however, underestimates the experimental results by a factor of 1.5.

An exact method for the computation of the attenuation due to water vapor for frequencies above 30 GHz is not available. Computations made for frequencies below 30 GHz using either the Van Vleck, Weisskopf or the kinetic theory line shape are in near agreement. Figs. 1 and 2 show the composite attenuation due to water vapor and oxygen computed using the Van Vleck, Weisskopf line shapes and the appropriate linewidth constants. Fig. 1 gives the one-way zenith attenuation values between the listed start heights and the top of the atmosphere. The temperature profile required for the calculation of attenuation was taken from the July 45°-N latitude standard atmosphere given in the U. S. Standard Atmosphere, and the humidity profile was taken from a model developed by Sissenwine, Grantham, and Salmela [14]. Below 30 GHz, the computations provide a good estimate of typical zenith attenuations. Between 30 and 35 GHz, water vapor typically causes more

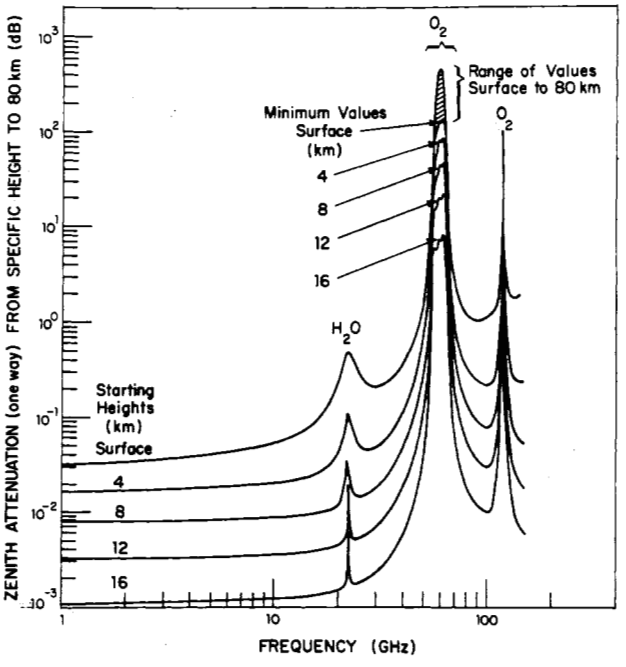

Fig. 1. Zenith attenuation versus frequency.

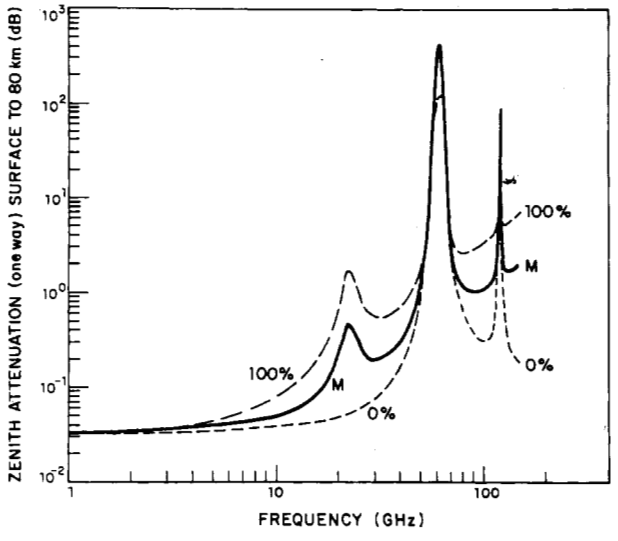

Fig. 2. Zenith attenuation versus frequency.

attenuation than oxygen and the curve may be in error as previously discussed. The zenith attenuation is, however, less than 0.3 dB and a factor of 3 error in the estimation of the attenuation coefficient provides less than a 0.6-dB error in the estimate of zenith signal strength. For a flat earth, the attenuation as a function of elevation angle is given by the zenith attenuation multiplied by the cosecant of the elevation angle. The cosecant law does not hold for elevation angles less than 6–10° due to earth curvature and refraction effects. Most satellite communication systems operate at elevation angles above 6° or a cosecant of 10. The maximum error introduced by using the above model for the computation of attenuation due to water vapor then is approximately 6 dB for frequencies in the 30–40-GHz range.

Frequencies between 40 and 80 GHz are mainly affected

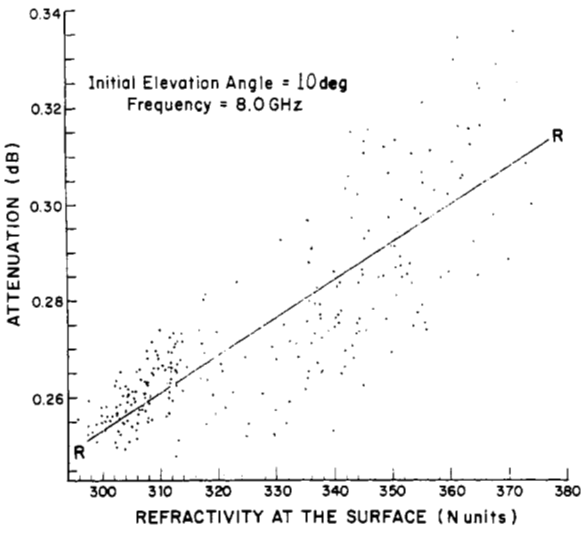

Fig. 3. Total attenuation at X band versus surface refractivity.

by oxygen absorption and the relative computation error introduced by the water vapor model is small. The curves show the minimum attenuation values that occur between the oxygen absorption lines. The top curve gives the zenith attenuation from the surface at the peak values of the stronger lines. Frequencies between 50 and 70 GHz, where the oxygen absorption is very high, have not been allocated for use by the satellite communication services. Allocations are proposed in the transmission "windows" between 80 and 110 GHz and between 125 and 150 GHz. In these windows water vapor attenuation is important but the models for computation are inadequate. The relative effects of water vapor are shown in Fig. 2. Both the 0 percent and 100 percent curves are fictitious in that the atmosphere is never completely dry nor saturated from the surface to the tropopause. The two dashed curves are for these two extreme cases and serve to illustrate the range of variation due to water vapor absorption.

The values of attenuation due to oxygen and water vapor will change with changes in meteorological parameters. Oxygen attenuation depends upon the pressure and temperature of the gas as a function of height. The temperature profiles are slowly changing with the effect that oxygen attenuation does not vary significantly from day to day. Water vapor attenuation depends both on the temperature profile and the amount of humidity in the atmosphere. Humidity is highly variable and changes rapidly in time and from place to place. The attenuation near the water vapor lines will be highly variable due to the variability of water vapor. The day-to-day variation at a frequency of 8.0 GHz is illustrated in Fig. 3. The data points are calculated by tracing rays through the atmosphere for an initial elevation angle of 10° using refractive index profiles computed from radiosonde soundings. The temperature and humidity profiles for each sounding were used to calculate the attenuation coefficient for points along the ray and the line integrals of attenuation coefficient along the ray were computed to give the attenuation. The data represent 273 radiosonde soundings made at Albany, N. Y., at 00 and 12Z for each day in February and August for the years 1966–1968. The dependence of the attenuation on the surface refractive index is shown. The peak-to-peak fluctuation nearly matches the change between the 0- and 100-percent curves of Fig. 2.

The atmospheric gases, water vapor, and oxygen are absorbers of microwave energy and, by the theory of radiative transfer, each elemental volume of the gas must emit energy in the microwave region of the spectrum to be in thermal equilibrium with the rest of the gas. Radiative transfer theory predicts that for a nonscattering medium [15]

$$I = \frac{\kappa k^2}{8\pi}\int_0^\infty T(s)\beta(s)\exp\left(-\int_0^s \beta(x)dx\right)ds \tag{1}$$

where

I = power per unit area per unit frequency per unit solid angle propagating along the ray in the $-s$ direction
k = wavenumber $= 2\pi/\lambda$, λ = wavelength
κ = Boltzmann's constant
$T(s)$ = kinetic temperature of the gas in degrees Kelvin at position s along the ray
$\beta(s)$ = attenuation cross section per unit volume of the gas at position s along the ray
$= A/10 \log e = A/4.34$ where A is attenuation coefficient in decibels per unit length.

An antenna observing the emitting medium would detect a received signal given by

$$\frac{P}{B} = \frac{\kappa}{4\pi}\int_0^{4\pi} G(\Omega)\int_0^\infty T(s)\beta(s)\exp\left(\int_0^s \beta(x)dx\right)ds\,d\Omega$$

where P/B is the received power per unit frequency, P received power, B receiver bandwidth, and $G(\Omega)$ the antenna gain function. Using the definition of antenna temperature,

$$T_A \triangleq \frac{P}{\kappa B} = \int_0^\infty\int_0^{4\pi}\frac{G(\Omega)}{4\pi}T(s)\beta(s)\exp\left(-\int_0^s\beta(x)dx\right)ds d\Omega$$
$$= \int_0^{4\pi}\frac{G(\Omega)}{4\pi}T_s(\Omega)d\Omega \approx \eta T_s(0) \tag{2}$$

where the sky temperature

$$T_s(\Omega) = \int T(s)\beta(s)\exp\left(\int_0^s\beta(x)dx\right)ds \tag{3}$$

and η = antenna efficiency.

Using the results of radiative transfer theory, the antenna temperature or sky temperature for a given antenna may be computed once the attenuation coefficient and the temperature of the gas is known as a function of position. Using the normal approximation of horizontal stratification, the sky temperature may be computed given the temperature and humidity profiles. Fig. 4 shows the results of a computation for several elevation angles together with measured values[1] of $T_s = T_A/\eta$. The computations were made using the Van

[1] Measurements by K. Wulfsberg [16].

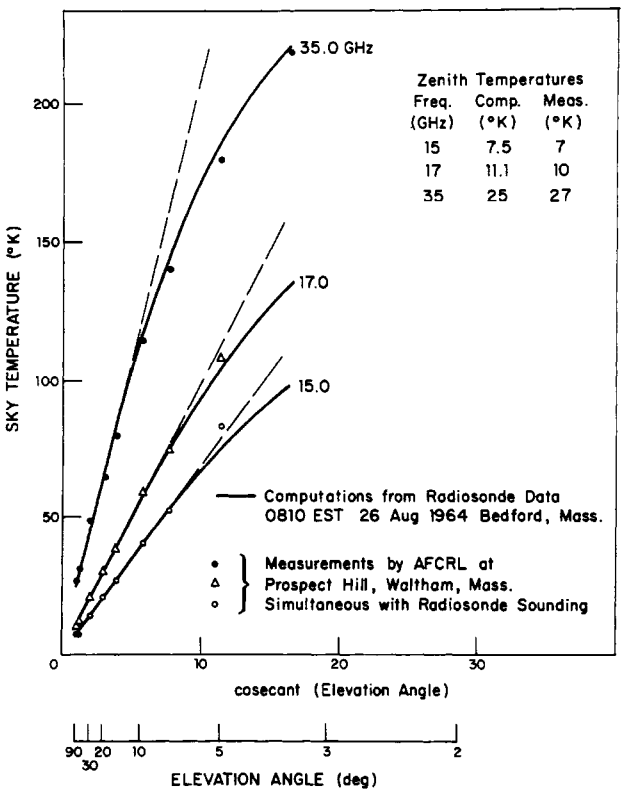

Fig. 4. Comparison between measured and computed sky temperature.

Vleck, Weisskopf line shape and the linewidths as discussed previously to provide an estimate of the attenuation coefficient and the integral of (3) was computed as a line integral along the ray using a ray tracing program that accounted for refraction effects. Good agreement is obtained at all elevation angles except the lowest at 15 and 17 GHz. The point of departure between the measured and calculated data occurred when the close-in sidelobes began to intercept the earth's surface. The 35-GHz data show larger differences between measured and calculated results but not in the direction expected due to the inadequacy of the attenuation computation model. The errors as shown here are most likely those due to the limited accuracy of the humidity elements used in the radiosonde measurements. The dashed lines correspond to an approximation to (3) that assumes a cosecant law for the attenuation and a total attenuation less than 1 dB. With these approximations, (3) becomes

$$T_s = T_s(0) \simeq T_E \int_0^\infty \beta(s) \exp\left(\int_0^\infty \beta(x)dx\right)ds$$

$$= T_E\left(1 - \exp\left(\int_0^\infty \beta(x)dx\right)\right)$$

$$= T_E \int_0^\infty \beta(x)dx \simeq T_E \cos(E) \int_0^\infty \beta(h)dh.$$

It is seen from Fig. 4 that the cosecant form of the approximation works well for elevation angles (E) above 10° for 15 and 17 GHz and above 15° at 35 GHz.

Molecular absorption is accompanied by anomalous dispersion. The anomalous dispersion causes small refractive index changes at frequencies close to the absorption lines. The refractive index changes are very small in the bands proposed for allocation to the satellite communications service and no bandwidth limitation is expected. The approximate expression for the refractivity N [17] may be used with negligible error up to a frequency of 50 GHz and, as an approximation may be used in the 70–150 GHz-region [18].

Rain Scattering

Individual hydrometeors such as rain, hail, and snow particles both absorb and scatter the incident radiation. The interaction between a particle and the incident field may be computed using electromagnetic scattering theory. Exact solutions are available only for simple shapes and distributions of the dielectric properties of the scatterer within the scatterer. Rain may be reasonably modeled using spheres and assuming the water to be a homogeneous lossy dielectric. More exact models of rain that take into account the nonspherical nature of the raindrops have been tried [19] but are only partially successful and useful only at low rain rates. Approximate calculations of hail and snow scattering have also been made. The problem of rain scattering has, however, received the most attenuation and, from the point of view of both probability of occurrence and severity of effect, it is the most important of the hydrometeor scattering phenomena.

The theory of scattering by a single lossy dielectric sphere of size comparable to a wavelength is based upon a series solution to the scattering problem [20]. The solution which is due to Mie has been verified experimentally many times (see for example Gerhardt, Tolbert, Brunstein, and Bahn [21]). The use of the scattering properties of a single raindrop in the description of the effects of rain also requires a description of the drop-size distribution and an assumption about the statistics of drop location within a volume. The use of measured drop-size distributions and the assumption that the drops are distributed throughout the volume in accordance with a Poisson process allows one to compute the per unit volume attenuation and scattering cross sections of rain [22]. Computations of the attenuation cross section per unit volume or the attenuation coefficient made using the average measured drop-size distribution reported by Laws and Parsons [23] are given in Fig. 5. For comparison, the attenuation coefficients for liquid water clouds are also presented. The cloud computations were made in an identical manner to those for rain except that the cloud particle size distributions of Weickmann and aufm Kampe [24] were used.

A complete description of the attenuation coefficient for hydrometeors would include the effects of snow, wet snow, hail, etc. For some of the scatterers, approximate computations may be made given their shape, orientation, and a description of their dielectric properties. For some scatterers, such as large misshapen wet hailstones, empirical measurements of their scattering properties are required. For each of the nonliquid scatterers, their size, orientation, and dielectric property distributions are unknown. The effects of snow are generally ignored since the attenuation

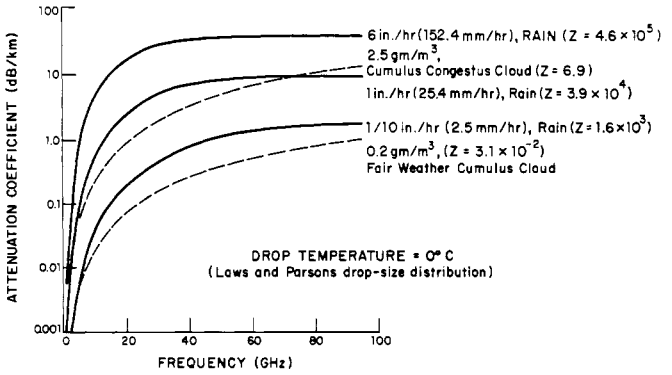

Fig. 5. Attenuation coefficient for liquid-water scatterers.

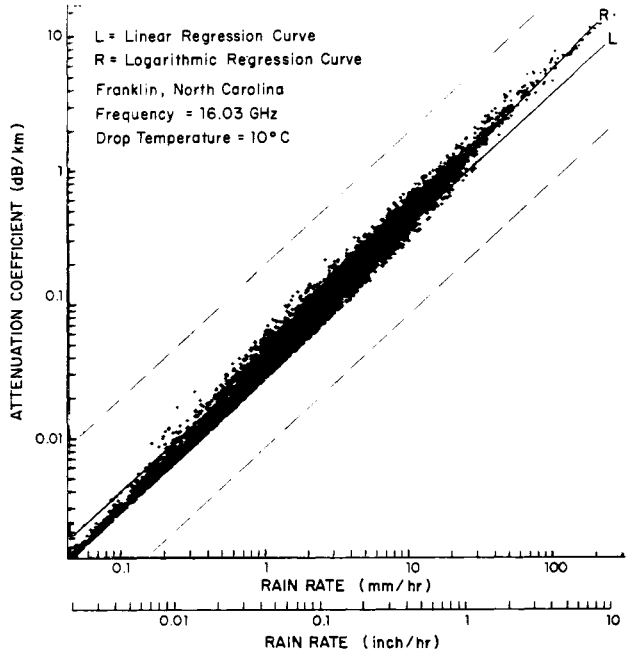

Fig. 6. Scattergram of attenuation coefficient versus rain rate, 16 GHz.

of snow is small in comparison with rain. The same is true of dry sleet and hail. Wet hail and melting snow may be modeled as very large raindrops. Their presence in rain will change the curves presented in Fig. 5 but, since little data are available about their effects, they will be ignored. It is only noted that hail and melting snow as present in the bright band or melting layer will cause departures from the rain models developed later. When the departures can be significant, they will be noted. The nonspherical scatterers cause polarization-dependent attenuation. Oguchi [19] has made approximate computations of attenuation due to rain for both vertical and horizontal polarizations. These computations show that less than a 20-percent difference exists between the two values of a given rain rate for rates and frequencies of interest. Since the difference is small in comparison with the statistical variation of attenuation at the same rain rate and frequency, the problem will be ignored. It is important only when the polarization properties of the transmitted signal are important as in polarization-diversity communication systems.

Measurements of raindrop size spectra show large variations for the same location, rain type, and rain rate. These

TABLE I
ATTENUATION VERSUS RAIN-RATE MODELS
$A = \alpha R^{\beta}$

Frequency (GHz)	Logarithmic α	Logarithmic β	rms error (percent)	linear ($\beta = 1$) α	rms error (percent)
2.8*	0.000459	0.954			
7.5	0.00459	1.06	28	0.00481	31
9.4	0.00870	1.10	30	0.00932	36
16.0	0.0374	1.10	22	0.0403	28
34.9	0.225	1.05	10	0.234	12
69.7*	0.729	0.893			

Models computed from 4741 data points using Franklin, N. C., [25] drop-size measurements, R in mm/h and A in dB/km.

* Data taken from computations by Mueller and Sims [26] using 4590 drop-size measurements.

variations imply that the attenuation and scattering properties of rain will also vary. Fig. 6 shows a scattergram which presents the results of computations of the attenuation coefficient and rain rate for 4741 drop-size distributions taken from December 1960 to March 1962 at Franklin, N. C., [25]. The dashed lines indicate the maximum and minimum possible attenuation coefficient for a given rate assuming the worst and best possible monodisperse drop-size distributions with the limitation that the drop size lie within the range of sizes attributable to rain. It is noted that the line positions depend on the limiting drop sizes used to define those allowable in rain. It is evident that, in natural rain, the fluctuations in attenuation due to variations in the drop-size distribution are significantly less than those theoretically possible. The rms variation in the data points about the linear least square fit or linear regression curve at a fixed rain rate is 28 percent, the rms variation about the logarithmic regression line is 22 percent, and the maximum theoretically possible error for a monodisperse distribution is 300 percent. At rain rates above 0.5 in/h, the linear fit departs from the data. For use in estimating attenuation for space communication applications, a least square linear fit to the data points corresponding to rates greater than 0.5 in/h would provide both a model that is easy to use and that fits the data as well as the logarithmic regression model. The logarithmic regression model, although fit to all the rain data, provides a reasonable fit to the data above 0.5 in/h.

The statistical analysis of many drop-size distributions provides models for use in calculating attenuation effects. The models are easier to use than the standard table of results of computations made using averaged drop-size distributions and have the advantage of providing an estimate of the possible variation in the estimated attenuation. Linear and logarithmic regression models for several frequencies are listed in Table I. The data for North Carolina reasonably represent the data for other climates in that the models deduced from the North Carolina data do not differ significantly from those computed using drop-size data from other areas [27]. Using the models given in Table I, the attenuation coefficients for a 4-in/h rate are given in Fig. 7 together with the values computed using the Laws and Parsons drop-size distribution and the Marshall and

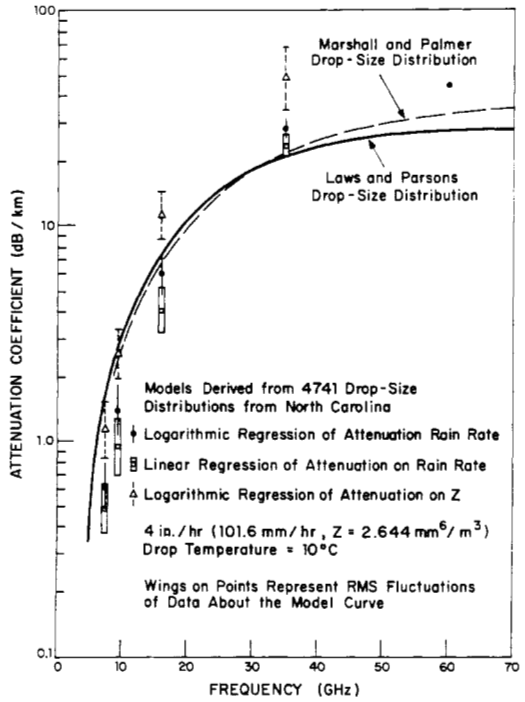

Fig. 7. Model estimates of attenuation coefficient versus frequency.

Palmer drop-size distribution [28]. The scattergrams for each of the frequencies show that for frequencies below 35 GHz and at the 4-in/h rain rate, the logarithmic regression model provides a better fit to the data than either of the averaged drop-size distributions. At 35 GHz, the linear model provides a fit that is as good as either of the averaged distributions.

The results for frequencies above 35 GHz depend critically on the number of small drops, with diameters less than 2 mm, that are represented in the model. The Marshall and Palmer model is a simple exponential drop-size distribution with more small drops than given in the Laws and Parsons distribution. The number of small drops, although not significant to either the calculation of rain rate or attenuation coefficient below 35 GHz, is significant in the calculations of attenuation at frequencies above 35 GHz. The drop-size camera used by the Illinois State Water Survey in making the size spectra measurements [29] unfortunately does not adequately measure the number of small drops due to the air flow about the camera housing. Other instruments show varying numbers of small drops for the same rain rate. The Joss [30] spectrometer shows a significant increase in the number of small drops in comparison with the camera data. A relative lack of small drops in the data used to compute the attenuation coefficient will cause the attenuation coefficient to be underestimated at frequencies above 35 GHz. Although the logarithmic regression model overestimates the available data at the 4-in/h rate, it may provide the best estimate of the attenuation. At present, better measurements of drop-size spectra at small drop sizes are required to improve the estimate of attenuation at frequencies above 35 GHz.

Both the model computations and the computations based upon averaged drop-size distributions provide an estimate of the attenuation coefficient. This is, however, not sufficient to compute the attenuation for a line-of-sight path through rain. Rain both scatters and absorbs the incident radiation. The scattered radiation may be multiply scattered and eventually reach the receiving antenna. For incoherent transmission systems, the radiative transfer equation governs propagation through the absorbing and scattering medium. The radiative transfer equation may be expressed as an integral equation in the form

$$\bar{I}(\boldsymbol{r}, \Omega) = \bar{I}_0(\Omega) \exp(-\tau(\rho, 0)) + \frac{1}{4\pi}\int_0^{\rho}\int_0^{4\pi} \omega\beta\bar{\boldsymbol{P}}(\Omega', \Omega) \cdot \bar{I}(\boldsymbol{r}', \Omega') \exp(-\tau(\rho, \rho'))d\Omega'\, d\rho' + \int_0^{\rho}(1-\omega)\beta\bar{B}(\boldsymbol{r}') \exp(-\tau(\rho, \rho'))\, d\rho' \quad (4)$$

where

$\bar{I}$ = Stokes vector form of I given in (1). The vector form is used to account for polarization effects.

$$\tau(\rho, \rho') = \int_{\rho'}^{\rho} \beta(x)\, dx$$

ρ = position along the ray measured from the far side of the medium

ω = single scattering albedo, the ratio of energy scattered to energy lost through both scattering and absorption

$\bar{\boldsymbol{P}}$ = phase matrix which describes bistatic scattering

$\bar{B} = (k^2T/8\pi)\{1, 0, 0, 0\}$ and is the Stokes vector for thermal emission.

For a nonscattering medium, the albedo ω is zero and

$$\bar{I}(\boldsymbol{r}, \Omega) = \bar{I}_0(\Omega) \exp(-\tau(\rho, 0)) + \int_0^{\rho} \beta\bar{B}(\boldsymbol{r}') \exp(-\tau(\rho, \rho'))d\rho'. \quad (5)$$

The first term on the right-hand side represents the attenuation for a source beyond the medium and the second term, the emission process as given in (1) which is the Stokes vector intensity component of (5) for the case of no source, $\bar{I}_0 = 0$ (note that s and ρ have different definitions). When the first term on the right-hand side is much larger than the second, the normal transmission equation results for propagation through a nonscattering attenuating medium.

When the single scattering albedo is not zero, the integral equation (4) must be solved for $\bar{I}$. For ω small, a Born series may be used to solve the equation. The first Born approximation is found by replacing $\bar{I}$ in the right-hand side by the value obtained when $\omega = 0$ as given by (5). For the case where the thermal emission is negligible in comparison with the energy from the source or for a communications link with a high signal to atmospheric noise ratio, the first Born approximation is given by

$$\bar{I}'(\boldsymbol{r}, \Omega) = \bar{I}_0(\Omega) \exp(-\tau(\rho, 0)) + \frac{1}{4\pi}\int_0^{\rho}\int_0^{4\pi} \omega\beta\bar{\boldsymbol{P}}(\Omega', \Omega) \cdot \bar{I}_0(\Omega') \exp(-\tau(\rho', 0)) \exp(-\tau(\rho, \rho'))d\rho'\, d\Omega'. \quad (6)$$

For an incident plane wave

$$\bar{I}_0(\Omega) = \bar{I}_0\delta(\Omega_0 - \Omega)$$

and

$$\bar{I}'(r, \Omega) = \bar{I}_0\delta(\Omega_0 - \Omega)\exp(-\tau(\rho, 0)) + \frac{1}{4\pi}\int_0^{\rho}\omega\beta\bar{P}(\Omega_0, \Omega) \cdot \bar{I}_0 \exp(-\tau(\rho', 0) - \tau(\rho, \rho'))d\rho'.$$

This solution may be evaluated if it is assumed that ω and $\bar{P}$ are constant throughout the rain volume. With this assumption,

$$\bar{I}'(r, \Omega_0) = \bar{I}_0 \exp(-\tau(\rho, 0)) + \frac{\omega\bar{P}(\Omega_0, \Omega_0) \cdot \bar{I}_0\tau(\rho, 0)}{4\pi} \cdot \exp(-\tau(\rho, 0)).$$

Considering only the intensity component of the Stokes vector and taking only the diagonal term of the $\bar{P}$ matrix, the approximate solution may be given as

$$\bar{I}(r, \Omega_0) = \bar{I}_0 \exp(-\tau(\rho, 0))\left[1 + \frac{P\omega\tau(\rho, 0)}{4\pi}\right].$$

For frequencies in the 1 to 150 GHz region and rain or cloud particle distributions, $P/4\pi \leq 1$ and the transmission equation for a nonscattering medium is obtained when $\omega\tau(\rho. 0) < 1$.

The single scattering albedo is readily computed for a given drop-size distribution using Mie theory [22]. The results obtained using the Laws and Parsons drop-size distribution are given in Fig. 8. For rain, the single scattering albedo is less than 0.6 and at frequencies below 10 GHz it is less than 0.1. At the lower frequencies where the total attenuation is low, it is expected that the nonscattering medium transmission equation will be sufficient. At higher frequencies, multiple scattering should be important. Using the criterion

$$\omega\tau(\rho_m, 0) = \omega\beta\rho_m = \frac{\omega A\rho_m}{4.34} < 1 \qquad (7)$$

where ρ_m is the distance at which multiple scattering becomes important, the distance ρ_m may be computed for a given drop-size distribution. The results of computations using the Laws and Parsons distribution are given in Fig. 9. The computations show that in rain and frequencies above 20 GHz, multiple scattering effects will be important. The criterion (7) was developed by comparing the first Born solution to the integral equation for radiative transfer with the transmission equation for a nonscattering medium. By comparing successive Born approximations, an identical criterion may be established for the use of the first Born approximation. When the criterion is not met, many terms in the Born series are required to find an answer.

Multiple scattering does not affect coherent transmission systems in the same way as incoherent systems. Except for scattering by drops spaced closer than a wavelength, the multiple scattered signals have random phases when compared with the attenuated direct signal. Since the drops are separated by distances larger than a wavelength the effect

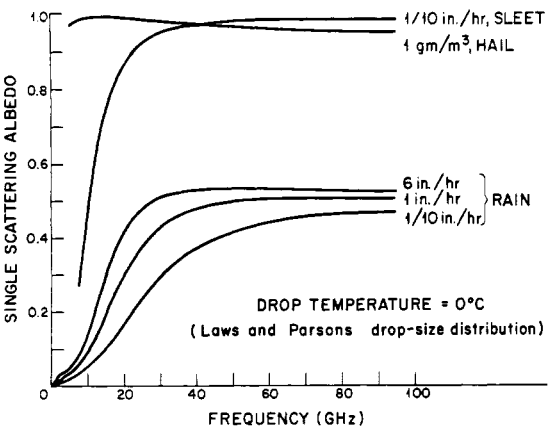

Fig. 8. Single scattering albedo versus frequency.

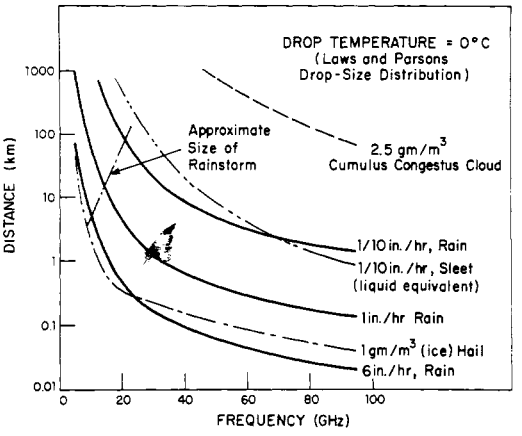

Fig. 9. Distance to multiple scattering versus frequency.

of multiple scattering on the attenuation of the coherent signal is negligible [22]. The transmission equation for a nonscattering medium, therefore, applies to coherent transmission systems for all combinations of ω and $\tau(\rho, 0)$. The multiply scattered signal is, however, present in the receiver as a form of noise of strength given by $\bar{I} - \bar{I}_0\exp(-\tau(\rho, 0))$. The effect of multiple scattering on an incoherent transmission system is to increase the received signal when compared to that predicted using the transmission loss equation for a nonscattering medium and to introduce multipath delay since the multiply scattered signal is delayed with respect to the direct signal. The attenuation experienced by an incoherent transmission system, therefore, should be less than that for coherent systems. Conversely, the effective bandwidth of a coherent system should be greater than for an incoherent system. At present, neither adequate measurements nor an adequate theoretical treatment of multiple scattering effects have been made. The computations of attenuation using the calculated attenuation coefficients as reported in the literature are all made using the transmission equation for a nonscattering medium and strictly apply only to coherent transmission systems.

The first comprehensive tabulation of the attenuation coefficient versus rain rate for a large number of frequencies in the centimeter and millimeter wavelength bands was made by Ryde and Ryde [31]. With the advent of the Ryde and Ryde tables, a series of measurements were performed

to verify their applicability. Goldstein [32] summarized the experimental work performed during World War II and noted that, except for the work of Anderson, Day, Freres, and Stokes [33], the experimental results tended to confirm the theory. The experimental data consisted of incoherent attenuation measurements made in natural rainfall over surface paths and simultaneous rain-rate measurements made along the path. The measurements tended to be crude and large variations in attenuation for a particular path averaged rain rate were reported. Due to the large variation in results, confirmation could only be inferred from the tendencies of the data. The work of Anderson, Day, Freres, and Stokes, however, did not show agreement between measured and estimated attenuations. Their results gave attenuations higher than those theoretically possible using a monodisperse drop-size distribution. Goldstein warned against accepting the work of Anderson, Day, Freres, and Stokes as evidence that the assumptions used in the estimation of attenuation were incorrect due to possibilities of error in the interpretation of the meteorological data.

Recently, Medhurst [34] corrected and extended the earlier work of Ryde and Ryde and compared the updated attenuation versus rain-rate curves with the experimental data then available in the literature. A number of additional measurements were available for comparison with the calculated results. The results of the comparison did not, however, validate the method. Medhurst observed a "marked tendency for the observed attenuations to fall *well above* levels which, according to the theory, cannot be exceeded." From this he concluded that "the applicability of Mie theory to the practical rainfall situation cannot be said to be demonstrated." Since the publication of Medhurst's paper, several additional experiments have been performed and reported [35]–[45]. Except for the work of Semplak and Turrin [42], each of the papers reported the same tendencies as Medhurst noted. Generally, at rain rates less than about 0.5 in/h, the measured attenuation exceeded the estimated attenuation and often the maximum possible attenuation using a monodisperse drop-size distribution and a path averaged rain rate. At higher rain rates, agreement was obtained between measurement and prediction based upon a suitable path averaged rain rate.

The measurements cited in the previous paragraphs and those reviewed by Medhurst tend to be crude in the handling of meteorological data. Generally, long paths were used with relatively few rain gauges. The only data that show good agreement between estimated and measured attenuation were published by Usikov, German, and Vakser [46]. In this work, an extremely short 50-meter path was used and the only data presented were for times when the rain rates reported by two gauges 30 meters apart and along the path were identical. The tendency toward agreement in experiments with short paths and dense rain-gauge networks and differing amounts of disagreement in others suggests that the discrepancies are not due to the inapplicability of Mie theory as suggested by Medhurst but due to an inadequacy in the use of meteorological data. The measurements were made using incoherent transmission systems and the tendencies of the results are toward too much measured attenuation rather than too little as would be expected when the simple transmission equation for a nonscattering medium is used. A physical description of rain shows that rain is composed of many small relatively intense showers imbedded in a larger area of light rain. For a network of rain gauges far apart, the showers would tend not to pass over the gauge but would intercept the line-of-sight. The showers which cause most of the attenuation would cause a comparison of estimated and measured attenuation to have too high a measured attenuation at the low path averaged rain rates where the showers missed the gauge and agreement at high rain rates when the shower is over the gauge.

The problem of measuring the intensity of rain with a sufficiently high spatial resolution to make an adequate prediction of attenuation for comparison with measured attenuation requires sensors different from the normal point rain gauges. High resolution radar measurements provide the required measurement capability and have the advantage of being able to measure rain intensity aloft along lines-of-sight typical of satellite communication systems. Using Mie theory, measured drop-size distributions, and the assumption about drop location within a volume, the backscatter cross section per unit volume of rain may be computed. Models then can be generated relating attenuation coefficient and backscatter cross section per unit volume using either the averaged drop-size distributions or statistical models based upon a large number of drop-size distributions. For radars operating at frequencies below 10 GHz, the backscatter cross section per unit volume may be estimated using the Rayleigh approximation.

$$\beta_B = \frac{\pi^5}{\lambda^4}|K|^2 Z$$

where

β_B = backscatter cross section per unit volume
$|K|^2$ = a function of the dielectric constant or liquid water, typically near 1
$Z = \sum nd^6$ where d is drop diameter and n is the number of drops per unit volume with diameter d.

Z is a meteorological parameter which depends only upon the size and number density of drops in a volume of rain. The radar measurements of backscatter cross section per unit volume provide an estimate of the meteorological parameter Z. The backscatter cross section at any frequency may also be described in terms of an effective Z value Z_e defined by

$$Z_e \triangleq \frac{\lambda^4 \beta_B}{\pi^5 |K|^2}$$

$$\simeq 3.5 \times 10^7 \lambda^4 \beta_B \,\mathrm{mm^6/m^3}, \quad \text{with } \lambda > 3 \text{ in cm}; \beta_B \text{ in } m^{-1}.$$

The scattergram for attenuation coefficient versus Z is given in Fig. 10. The logarithmic regression provides a

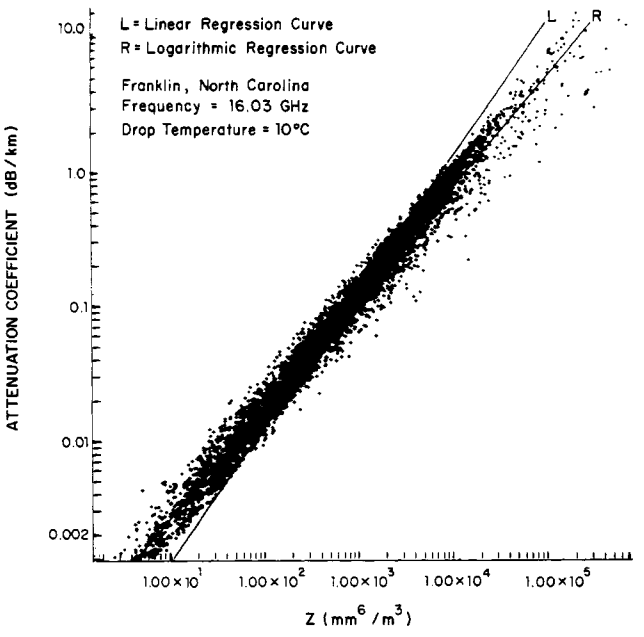

Fig. 10. Scattergram of attenuation coefficient versus Z, 16 GHz.

TABLE II
ATTENUATION VERSUS RADAR REFLECTIVITY FACTOR MODEL
$A = \alpha Z^{\beta}$

Frequency (GHz)	α	β	rms error (percent)
7.5	0.0000573	0.792	35
9.4	0.0000929	0.819	30
16.0	0.000383	0.824	29
34.9	0.00315	0.772	41

Models computed from 4741 data points using Franklin, N. C., [25] drop-size measurements, Z in mm^6/m^3 and A in dB/km.

reasonable estimate of the attenuation coefficient at the higher rain rates or Z values even though the entire set of drop-size data was used to calculate the regression coefficients. The linear regression does not provide a reasonable fit. Table II gives the model coefficients for the logarithmic regression at several frequencies. Using the model data and a Z value of 2.6×10^5 mm^6/m^3 which is equivalent to a 4-in/h rain rate using the Laws and Parsons drop-size distribution, the attenuation was computed for comparison with the other model computations given in Fig. 7. The results show good agreement with the averaged drop-size models at frequencies less than 10 GHz and an apparent overestimation of attenuation at the higher frequencies. Better results would have been obtained if only the data corresponding to rain rates above 0.5 in/h were used in the regression analyses. Although Z is proportional to the sixth power of the drop diameter and the attenuation coefficient and rain rates are approximately proportional to the third power of the drop diameter, sufficient statistical regularity is obtained in the drop-size distributions to cause the rms fluctuations of the data points about either the rain rate or Z value derived models to have the same order of magnitude.

The estimation of the attenuation properties of rain using radar data requires that no hail, sleet, or snow be present in the radar resolution volume. As shown in Fig. 8, the scattering albedo of ice particles is nearly unity and the attenuation for a given backscatter cross section is lower for ice particles than for wet ice or liquid water particles. In normal weather radar practice, two situations may occur when radar estimates of attenuation based upon the model previously discussed are in error. In widespread light rain, a bright band of several thousand foot thickness generally will be evident. This is a thin layer of melting snow which shows up as a region of enhanced signal both due to the large size of the wet snowflake and to its slow fall speed relative to that of the liquid drop of the same mass of water. Above the bright band, snow is present which may have a scattering cross section nearly equal to that of the rain below the bright band but which has negligible attenuation. As an approximation, the rain model may be used to relate the Z_e values below and in the bright band to the attenuation coefficients in those locations and the snow above the bright band may be assumed to produce no attenuation. Hail manifests itself as a small area of extremely high scattering cross section with Z_e values sometimes reaching 10^7. The effect of the modeling process is to generate an overestimate of the attenuation coefficient for the radar resolution cells containing the hail returns. As a guide line, hail often is present in volumes that have a Z_e value greater than $10^{5.5}$. For Z_e values of $10^{5.5}$ and lower the use of the modeling equation to predict attenuation may be assumed to produce the results discussed before.

A radar measurement of the structure of a New England summer shower is shown in Fig. 11. The radar used was the Millstone Hill L-band radar which has approximately 1 km^3 resolution volume [27]. The radar map of rain intensity shows several small cells with 10-dB down widths the order of 5 km across and peak to minimum rain intensity distances the order of 3 km. The rate tabulated along with the Z_e values is computed from Z_e using the approximate expression $Z_e = 200\ R^{1.6}$ which is the standard relationship used by radar meteorologists. Attenuation coefficient estimates are also tabulated. These are based upon a logarithmic regression analysis of Miami drop-size data [47]. Using the model and calculating the attenuation along the ray from the radar site through the shower cells, the attenuation estimate given in Fig. 12 results. The dots are the estimated values and the lines include the plus and minus rms fluctuations due both to uncertainties in the radar measurements and the fluctuations in the drop-size data. From these data it is seen that the significant amounts of attenuation are contributed by small areas of rain, usually less than 5 km in extent.

Rain cells of the intensity shown on Fig. 11 usually extend to about 8 km height in New England. Since the cells have nearly equal heights and horizontal extents, the attenuation contributed by one of the cells along a line-of-sight will be the same for the elevated path between a ground terminal and satellite as it is at the very low elevation angle

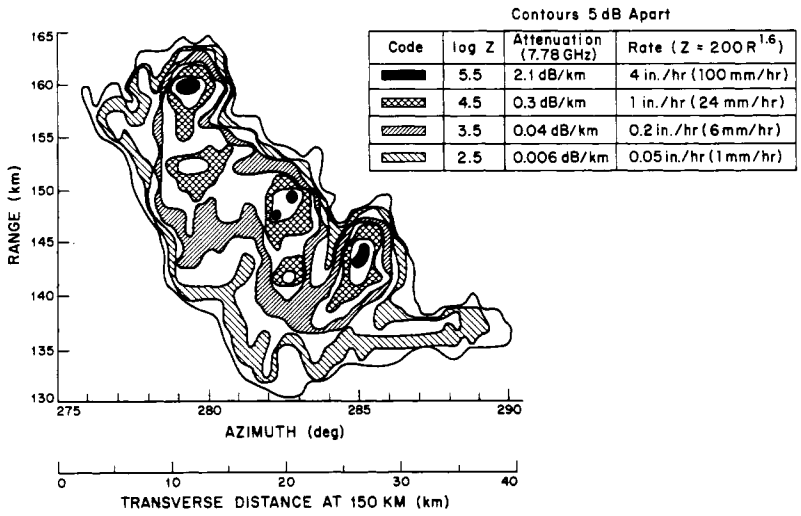

Fig. 11. Weather radar map for New England showers.

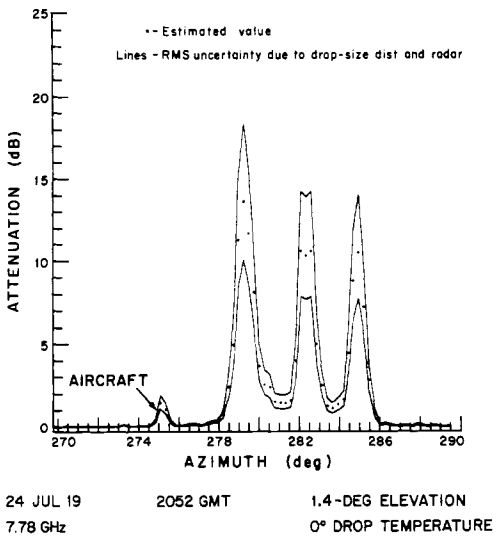

Fig. 12. Estimated attenuation using Millstone Hill L-band radar data.

used in the radar measurements. For satellite communication applications, it is seen that attenuations at X band of the order of 15–20 dB may be encountered when one of the showers intercepts the communications path. The probability of this happening for an elevated path confined to a fixed direction is small because of the small area occupied by the shower. A study of the occurrences of rain cells of sufficient intensity to cause 10-dB or higher attenuation at X band along a path with fixed azimuth was made by Austin [48]. She showed that for the years 1961 and 1962, 10 dB would be exceeded 1.3 h per year occurring on 5 separate days for a 20° elevation angle. This reduces to 0.4 h per year on 3 separate days for occurrences of attenuation with this severity for an elevation angle of 60°. At higher frequencies, and for coherent transmission systems, the attenuations would be higher. Using the Laws and Parsons data, the attenuation at 16 GHz should be 3 times that at 7.78. The peak attenuations would then lie in the 45–60 dB range. The attenuations for locations between the cells would be of the order of 5–10 dB. To get around the problems caused by the certain outage when the rain cell is along the path, space diversity schemes have been proposed [41] that rely on the use of two or more paths separated by more than a cell width. Using such a scheme, when the rain cell blocks one path, the attenuation on the other will be acceptable. The only difficulty here is that an insufficient amount of meteorological data is available from which to determine the optimum diversity distance. It is also noted that, as the frequency is increased, attenuations due to clouds and very light rain begin to cause unacceptable outages. In this case, the diversity distances may become unacceptably large since, at a fixed frequency, the size of the rain and cloud areas encompassing a given or higher attenuation coefficient increases as the attenuation coefficient decreases.

In an effort to verify the procedure used to estimate attenuation given the high resolution radar data, simultaneous measurements of antenna temperature caused by thermal emission from rain were made using a 7.78-GHz radiometer and the large Haystack antenna system [27]. The antenna temperature for rain may be computed using the first Born approximation to (4) for the case where $\bar{I}_0 = 0$ since the $\omega\tau(\rho, 0) < 1$ criterion is met for the rain showers at 7.78 GHz. The first Born approximation to (4) may be reduced to (1) in the limit that $\omega = \ll 1$. At 7.78 GHz, $\omega \sim 0.1$ and (1)–(3) were used to compute the expected antenna temperature. The computations used the attenuation coefficient found from the model, the measured radar backscatter cross section per unit volume, and the temperature of the raindrops deduced from a radiosonde sounding. The results are given in Fig. 13. Due to the limited dynamic range of the radar in comparison with the difference in cross section between rain and clouds, the clouds that contribute to the antenna temperature at azimuth angles be-

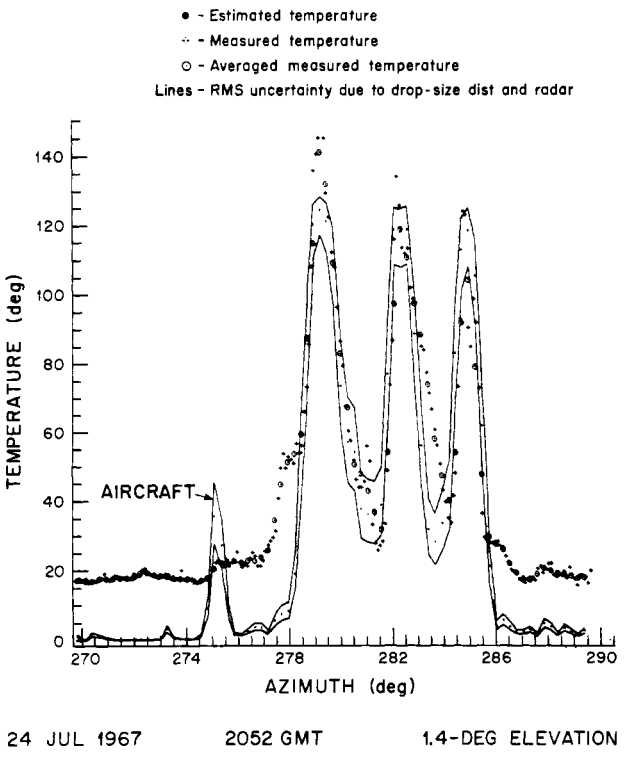

Fig. 13. Estimated and measured antenna temperature relative to a 2° elevation angle clear sky value.

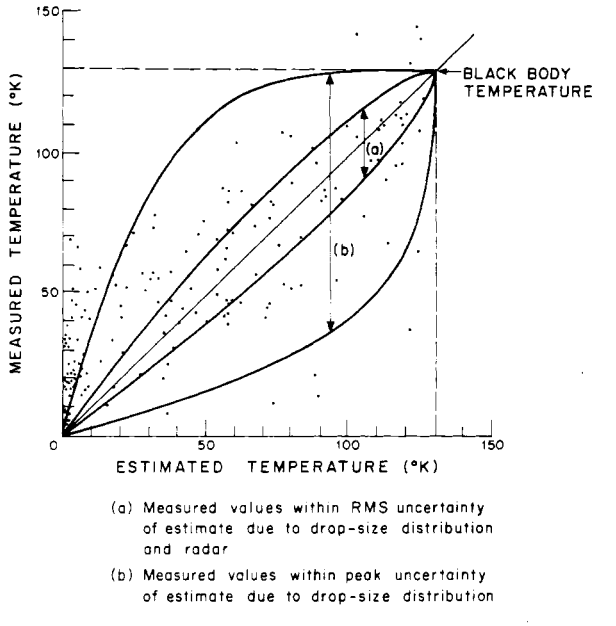

Fig. 14. Comparison between estimated and measured antenna temperature.

tween 270° and 274°, and 286° and 290° could not be detected. The comparison only applied at the peaks of the temperature versus the azimuth curve. Good agreement is observed except at the peak at 279° where the antenna temperature is higher than predicted. Fig. 14 shows the comparison between measured and estimated attenuation for all the azimuth scans made in the storm. Good agreement is obtained for rain when the estimated temperature change is in excess of 20°K. For lower estimated antenna temperatures, cloud effects dominate and no comparison may be made. A few points are above the line labeled blackbody temperature which is the maximum theoretically possible. These points correspond to the discrepancy shown in Fig. 13. They may be due to nonthermal emission from rain as proposed by Sartor and Atkinson [49]. The results given in Fig. 14 do not show the large discrepancies between attenuation estimation and measurement reported by Medhurst and workers since Medhurst. This is attributed to the use of the high resolution radar which measures a volume average of rain intensity and not a point surface flux measurement as given by rain gauges.

Although the dominant effect of rain on a line-of-sight path is to attenuate the signal, other effects are possible. A coherent transmission system may suffer bandwidth limitations if the bandwidth is sufficiently large due to the frequency dependence of the attenuation and phase shift introduced by the rain. A study of this problem by Crane [50] showed that the transmission bandwidths are in excess of 3.5 GHz for all situations likely to be encountered and, since the maximum total bandwidths allocated are of this order, no bandwidth limitation is expected. For incoherent transmission systems, a bandwidth limitation may result from the spread in time delays of the multiple scattered signal. No adequate study of this problem has been made. The meager amount of experimental data currently available [44], [45] seems to indicate that an outage due to excess attenuation will occur before a measurable bandwidth limitation occurs.

Rain scattering may also cause interference between ground systems operating at the same frequency and beyond each other's radio horizon. The phase function or the bistatic scattering cross section per unit volume normalized by the total scattering cross section per unit volume differs from that of a Rayleigh scatterer by less than an order of magnitude for the range of frequencies being considered. This implies that, for polarization perpendicular to the plane of incidence, the bistatic scattering process can be approximated as being isotropic and for polarization in the plane of incidence, the process can be modeled with the cosine squared scattering angle dependence. Since satellite communication systems often use circular polarization, the scattering process may be, to first order, approximated as isotropic. The bistatic scattering cross section per unit volume, therefore, may be assumed to be that measured by the radar and described by the parameter Z_e. This approximation may also be extended to scattering by snow and hail. Measurements of the bistatic scattering cross section of melting snow have, however, tended to show a significant enhancement in the forward direction [51]. For the prediction of interference, the radar-measured scattering cross-section together with the relevant geometry and antenna patterns are used to calculate the transmission loss. For frequencies above about 4 GHz, the attenuation of the signal as it propagates to and from the scattering volume must be

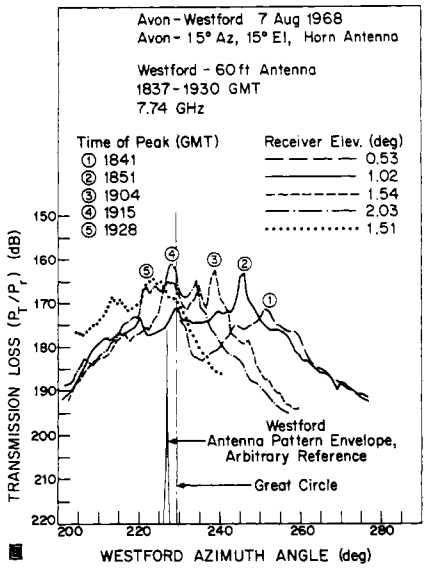

Fig. 15. Bistatic scattering measurements with rain.

included. At frequencies above 15–20 GHz, the full radiative transfer problem must be solved.

When compared with the other mechanisms of transhorizon propagation, rain scattering is of most concern mainly because the scattering cross section is nearly isotropic and significant amounts of energy may be coupled from one antenna to the other at large scattering angles. The other transhorizon propagation mechanisms are most efficient at low elevation angles and in directions along or close to that of the great circle path [52]. This implies that by providing suitable shielding at low elevation angles in directions close to that of the great circle path, all but the problems due to rain scattering may be mitigated. Rain scattering, therefore, provides the limiting case upon which coordination distances must be based.

Experimental measurements of bistatic scattering by rain were made at *X* band over a 145-km path between Avon, Conn., and the Westford Communications Terminal for comparison with the Millstone Hill *L*-band radar data to demonstrate the theory. A series of azimuth scans across the great circle path are presented in Fig. 15. For these measurements, a standard gain horn antenna was used to illuminate the rain and the Westford 60-ft antenna was scanned in synchronism with the Millstone radar antenna to gather bistatic scattering data. The measurements show the rain scattered signal off the great circle path to exceed the troposcattered signal along the great circle path. The horn antenna was pointed 34° to the north of the great circle path and was not directed toward the rain shower peaks labeled 3, 4, and 5. A comparison between the peak received signal and that computed from the Millstone radar measurements with allowance for rain attenuation show agreement to within the measurement accuracies of both the radar and bistatic scatter measurement system.

In this section, we have shown that, except for the effects of multiple scattering, both attenuation and interference levels may be adequately calculated given the description of rain intensity in space and time. For use in the design of satellite communication systems, it is not sufficient to be able to compute the effects given the physical description of rain. What is required is a statistical estimate of the probability of occurrence of specified attenuation or interference levels. These can only be computed when the probability of occurrence of a specified rain intensity is known for any point in space together with the conditional probabilities of both the volume occupied and time occupied by rain of the specified or greater intensity. The required statistics are climatological in nature, and with the current state of meteorological theory, must be provided from observational data. Unfortunately, there is no observational data. The only climatological data uniformly available in the United States are hourly rain-gauge summaries and excessive precipitation reports. The problem is to extract the required probability estimates from the available data. To do this meteorological models must be constructed to generate the required statistical data. Since the models will be an intermediate step between the meteorological data and the desired propagation statistics, measured propagation statistics must be obtained to establish the validity of the model.

The sun tracker measurements of Wilson [53], the ATS-V Millimeter Wave Experiment [44], and several surface path measurements [36], [41], [45], [54] are providing statistical data on attenuation at millimeter wavelengths. The statistical data will have their greatest use in validating and extending the models for estimating rain effects when they are available. The direct use of the statistical data from propagation experiments in the design of communication systems can, however, be dangerous since the long time sequences of data required for adequate estimation of the rare events of importance to the design of reliable communication systems are not available and since the design efforts often are not for the location at which the data were taken and the required climatological modification of the statistical data is not known.

Refraction Effects

The index of refraction of air depends upon temperature, pressure, and humidity and varies with changes in the meteorological parameters. Due to the approximately exponential decrease in atmospheric density with height, the refractive index generally decreases in an exponential manner with height. Local features such as high humidity gradients and temperature inversion layers lead to small height intervals in which the refractive index profile departs markedly from the general exponential decrease. To first approximation, the refractive index structure is horizontally stratified and the regions of departure from the exponential decrease appear as thin horizontal layers. The refractive index at a particular height will change slightly in an oscillatory manner due to internal waves and in a random manner due to turbulence. For line-of-sight propagation at elevation angles above 5° and for the frequency range of interest, the effects of internal waves and turbulence are second order.

The changes in refractive index with position cause rays propagating through the atmosphere to change their direction. Ray bending due to the averaged properties of the

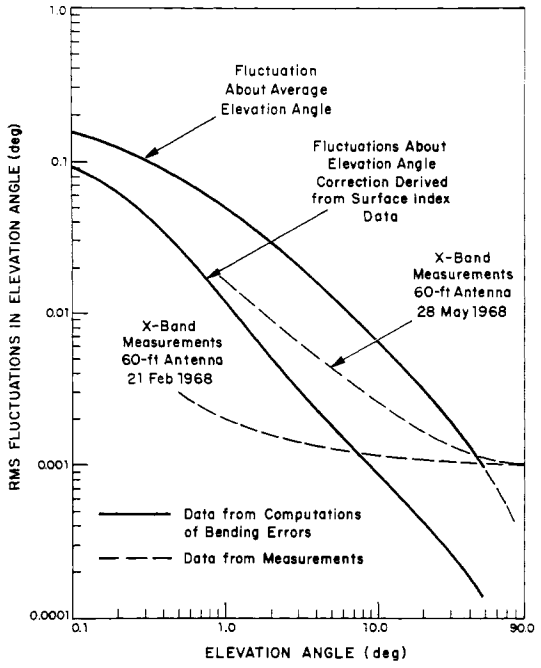

Fig. 16. Fluctuations in elevation angle due to atmospheric effects.

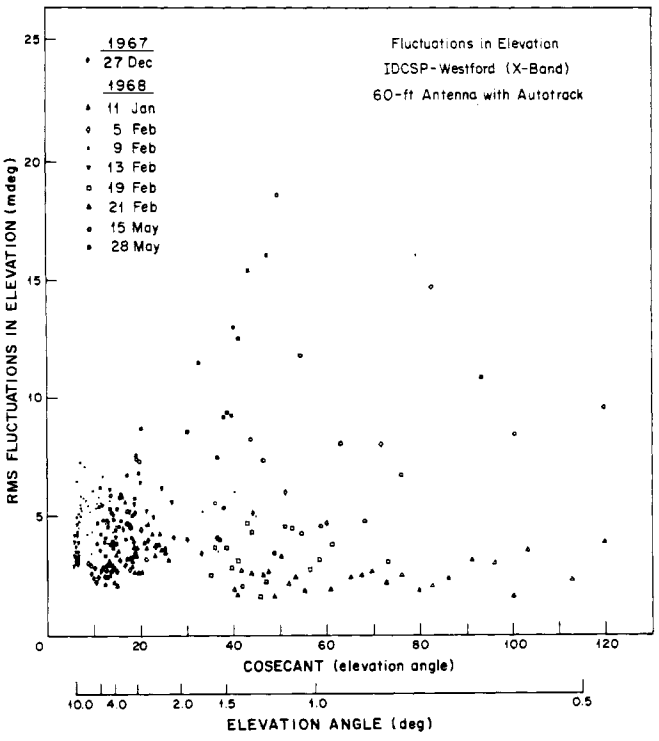

Fig. 17. Measured fluctuations in elevation angle at X band.

horizontal layers give rise to elevation angle pointing errors. These may be important to satellite communication systems operating at low elevation angles that have no way of tracking the apparent position of the satellite. Computations of the amount of bending experienced by a ray traversing the atmosphere were made using radiosonde data from Albany, N. Y. We used 273 refractive index profiles taken from the 00 and 12Z soundings on each of the days in February and August for the years 1966–1968. The rms fluctuation of the calculated values of bending about the average value and about the values predicted using a least square-fit linear dependence upon surface refractive index are presented in Fig. 16. The results show the day-to-day variation in apparent source position or the day-to-day change in elevation angle for a satellite which does not change in position relative to the ground terminal.

Both internal wave and turbulence caused fluctuations in the index of refraction will cause fluctuations in the apparent elevation and azimuth angles of the source. These effects may be important to nontracking antenna systems that operate at low elevation angles. Measurements made using the X-band beacon transmitter on the IDCSP satellites and the Westford Ground Terminal [55] of fluctuations in elevation about the smoothed apparent position of the satellite are shown in Fig. 17. Simultaneous measurements of azimuth angle fluctuations gave identical results. The winter measurements are of fluctuations caused by turbulence. The summer measurements show effects due both to turbulence and internal waves. Smoothed representations of one of the winter measurements and one of the summer measurements are shown in Fig. 16.

The changes in refractive index also cause changes in signal levels due to focusing and scattering. The attenuation due to focusing was computed for the 273 refractive index profiles from Albany. The results of the computations are shown in Fig. 18. From the computations, it is seen that

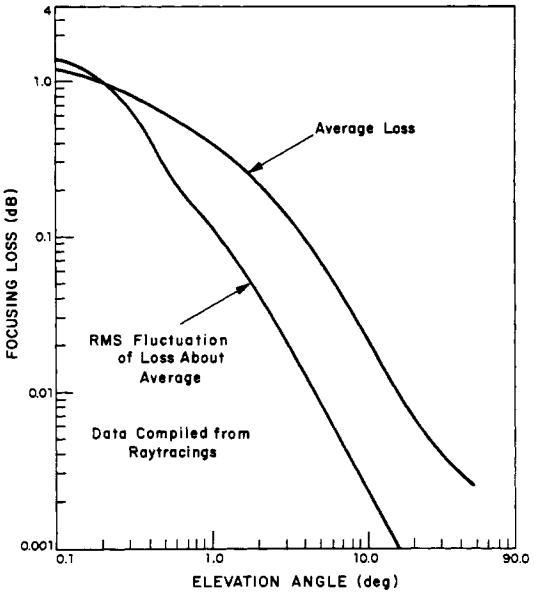

Fig. 18. Focusing loss due to atmospheric refraction effects.

focusing loss is less than 0.1 dB for elevation angles greater than 5° and may be neglected in comparison with the effects of molecular absorption and rain attenuation. Turbulence and internal waves also cause amplitude fluctuations. Measurements of amplitude changes made at X band using a 60-ft monopulse tracking antenna are shown in Fig. 19. The results again show summer and winter dependences. The amplitude fluctuations at X band are, however, negligible at the elevation angles of interest to satellite communications. It is noted that, at elevation angles below 5°, deep fading is observed in the summer months. The data show that the fades are often greater than 30 dB and, at other times, signal enhancements of 6 dB are measured. This is

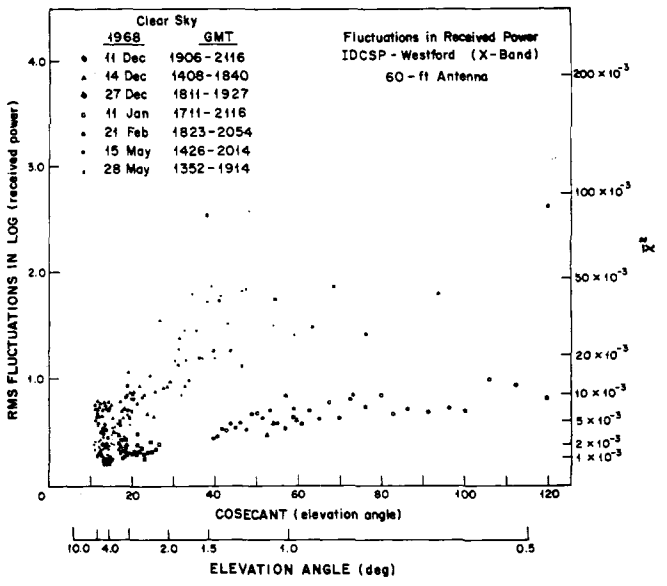

Fig. 19. Measured fluctuations in received power at X band.

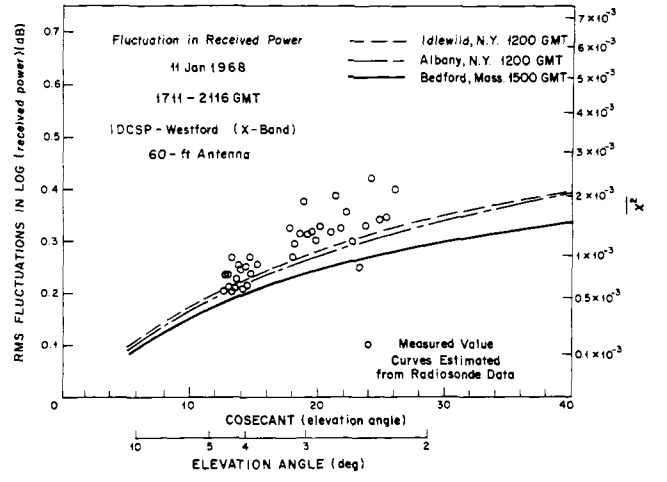

Fig. 20. Comparison between estimated and measured received power fluctuations at X band.

indicative of interference between two rays propagating from transmitter to receiver. A possible explanation of the deep fading phenomena is two-ray propagation through an internal wave structure.

Amplitude scintillations due to turbulence are predicted using the theory of propagation through a turbulent medium [56]. A comparison between measurements and an estimate based upon theoretical computations and a model for the computation of the intensity of turbulence as a function of height using radiosonde data [55] is shown in Fig. 20. The comparison shows reasonable agreement. Computations based upon the theory of propagation through turbulence indicate that the magnitudes of the phase and amplitude fluctuations are frequency dependent. The amplitude changes due to focusing by the averaged refractive index fluctuations are essentially independent of frequency in the region between 1 and 50 GHz since they are derived from the equations of geometrical optics. Computations of amplitude scintillations at frequencies higher than 8 GHz have been reported by Lane [57]. He computed that the

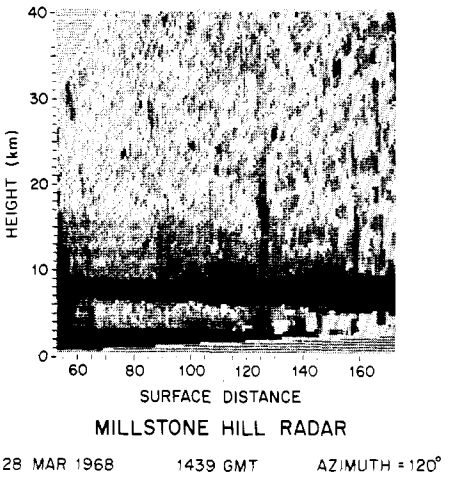

Fig. 21. RHI display. Millstone Hill L-band radar.

maximum amplitude fluctuation for a vertical line-of-sight through the atmosphere could be 4 dB at 100 GHz and 2.2 dB at 35 GHz. Janes, Thompson, Smith, and Kirkpatrick [58] have made measurements of both the phase and amplitude fluctuations at 9.6 and 34.5 GHz. Although the rms amplitude fluctuations were not reported, the ratios of the amplitude spectral densities are in agreement with the theory. The phase scintillation measurements at the two frequencies show identical behavior when expressed as percent of total phase along the path. This indicates that over the time scales used in the measurements, the phase fluctuations behaved as may be predicted by a statistical geometrical optics theory. Phase statistics are not readily computed using turbulence theory since they depend upon the intensity of turbulence with large scale sizes which are not modeled by the theory. Phase difference statistics for space or time positions close together are calculable by the theory. Lane also reports computations of phase difference variations which are in agreement with the measurements of Lee and Waterman [59].

The random fluctuations of refractive index associated with turbulence will cause scattering of the incident radiation. Scattering by turbulence may be detected by very sensitive radars. The bistatic scattering cross section per unit volume of turbulence is related to C_n^2, a measure of the intensity of turbulence in the inertial scale size subrange or scale sizes between approximately 0.01 and 100 meters [52]

$$\beta_\perp(\phi) = \frac{1.757 C_n^2}{\lambda^{1/3}} \left(\sin \frac{\phi}{2}\right)^{-11/3} \tag{8}$$

$$\beta_{||}(\phi) = \beta_\perp(\phi) \cos^2 \phi$$

where $\beta_\perp$ is the bistatic scattering cross section per unit volume for radiation polarized perpendicularly to the plane of scattering, $\beta_{||}$ for polarization in the plane of scattering, and ϕ is the scattering angle. For scattering by turbulence, (8) may be used to define an effective C_n^2 given the measured backscatter cross section per unit volume. An RHI display showing turbulent layers is presented in Fig. 21. From the figure, the regions of turbulent scattering appear as thin horizontal layers at heights up to 15.5 km. A composite of

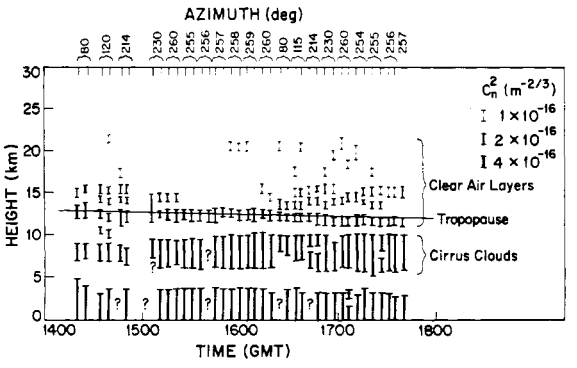

Fig. 22. Radar detected atmospheric layer structure for May 28, 1968.

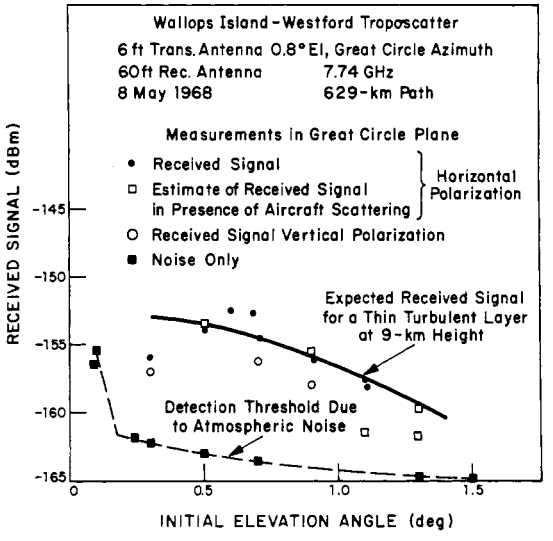

Fig. 23. Comparison of estimated and measured received signal versus elevation angle.

all the layer measurements for March 28, 1968 is shown in Fig. 22. From these data, it is seen that persistent scattering layers exist in the atmosphere. These layers are one of the dominant mechanisms for transhorizon scatter propagation. For scattering at low elevation angles along the great circle path, the scattering angle is small and the scattering cross section per unit volume becomes large. At the small scattering angles, the layers appear to be thin horizontal turbulent volumes for frequencies greater than about 2 GHz. For lower frequencies and at small scattering angles, the layers begin to appear as specular reflectors due to their thinness.

Experimental measurements of scattering by thin layers at heights above 6 km were conducted at 7.74 GHz over a 630-km path using a 6-ft transmit antenna at Wallops Island, Va. and the 60-ft Westford Communications Terminal as the receiver [60]. An elevation scan showing measured and predicted received signal strength based upon thin turbulent layer scattering is shown in Fig. 23. The figure shows that transhorizon scattering due to turbulent layers may be predicted when the layer structure is known. From estimates of the extremes of turbulent layer intensities, the interference field strengths may be computed. A comparison between the maximum field strengths due to turbulent scattering and due to rain scattering [52] shows that, for antennas pointed at elevation angles below 5° and within 5° of the great circle path, thin turbulent layer scattering can be most important. For all other antenna pointing angles, rain scattering is most important. The data shown in Fig. 15 show that rain was most important for that day even for pointing angles along the great circle path and elevation angles below 5°.

Strong gradients of refractive index near the surface may, when they are horizontally stratified and extend between the transmitter and receiver, cause ducted propagation over the horizon between the two terminals [32]. The field strengths that exist when this phenomenon occurs may exceed those for free space at the same distance. This phenomenon occurs quite often over the water and in coastal areas. It also may occur inland as well as along the coast, especially after the passage of cold-front showers. For unprotected stations, ducting will produce interfering signals far stronger than that due either to rain or to turbulent layer scattering. Coupling of energy into a duct, however, only occurs at low elevation angles, below 0.5–1°. This implies that site shielding such as terrain blockage at the low elevation angles or the existence of a series of hills along the path that would break up the layers causing the ducting would eliminate the problem.

Measurements made at 4.5 GHz on a 145-km path between Avon, Conn., and the Westford Communications Terminal have shown that with foliage shielding to 2.5° elevation angle and terrain shielding to 0.5° elevation angle in the direction of the great circle path, no enhanced signal was observed during periods of ducting when the radar detected ground echoes from the hill on which the scatter-link transmitter was sited. In a similar way, terrain diffraction, which can provide interference on short transhorizon paths, may be guarded against using site shielding techniques.

Summary

The review of propagation phenomena of importance to centimeter and millimeter wavelength band communication systems shows that rain causes the major difficulties. Rain attenuation at frequencies of 16 GHz and above may be so severe that diversity paths must be provided to maintain reliable communications. Rain scattering also provides the dominant mechanism for coupling energy between two well-sited systems operating at the same frequency and beyond each other's radio horizon. Techniques for computing the effects of rain are well in hand. The statistical properties of rain and from these the statistical properties of attenuation and interfering level fields are not well known. This together with an investigation of multiple scattering effects are the problems requiring the most effort at the present time.

References

[1] J. H. Van Vleck and V. F. Weisskopf, "On the shape of collision-broadened lines," *Rev. Mod. Phys.*, vol. 17, pp. 227–236, 1945.

[2] M. L. Meeks and A. E. Lilley, "The microwave spectrum of oxygen in the earth's atmosphere," *J. Geophys. Res.*, vol. 68, pp. 1683–1703, 1963.

[3] W. B. Lenoir, J. W. Barrett, and D. C. Papa, "Observations of micro-

wave emission by molecular oxygen in the stratosphere," *J. Geophys. Res.*, vol. 73, pp. 1119–1126, 1968.
[4] S. A. Zhevakin and A. P. Naumov, "The coefficient of absorption of centimeter and millimeter radiowaves in atmospheric oxygen," *Izv. Vyssh. Ucheb. Zaved. Radiofiz.*, vol. 7, 1964.
[5] *U. S. Standard Atmosphere Supplements*. ESSA, NASA, and the U. S. Air Force, U. S. Government Printing Office, Washington, D. C., 1966.
[6] G. E. Becker and S. H. Autler, "Water vapor absorption of electromagnetic radiation in the centimeter wavelength range," *Phys. Rev.*, vol. 70, pp. 300–307, 1946.
[7] A. H. Barrett and V. K. Chung, "A method for the determination of high-altitude water-vapor abundance from ground-based microwave observations," *J. Geophys. Res.*, vol. 67, pp. 4259–4266, 1962.
[8] J. H. Van Vleck, "The absorption of microwaves by uncondensed water vapor," *Phys. Rev.*, vol. 71, pp. 425–433, 1947.
[9] D. H. Staelin, "Passive remote sensing at microwave wavelengths," *Proc. IEEE*, vol. 57, pp. 427–439, April 1969.
[10] S. A. Zhevakin, V. S. Troitsiy, and N. M. Tseytlin, "Radiation of atmosphere and investigation of the absorption of centimeter radio waves," *Izv. Vyssh. Ucheb. Zaved. Radiofiz.*, vol. 1, 1958.
[11] S. A. Zhevakin and A. P. Naumov, "Absorption of centimeter and millimeter radio waves by the atmospheric water vapor," *Izv. Vyssh. Ucheb. Zaved. Radiofiz.*, vol. 6, p. 1327, 1963.
[12] E. P. Gross, "Shape of collision-broadened spectral lines," *Phys. Rev.*, vol. 97, pp. 395–403, 1955.
[13] W. S. Benedict and L. D. Kaplan, "Calculation of line widths in H_2O-N_2 collisions," *J. Chem. Phys.*, vol. 30, pp. 388–399, 1959.
[14] N. Sissenwine, D. D. Grantham, and H. A. Salmela, "Humidity up to the mesopause," in *Air Force Surveys in Geophys.*, no. 206 Air Force Cambridge Lab., Tech. Rep. AFCRL-68-0550, October 1968.
[15] S. Chandrasekhar, *Radiative Transfer*. Oxford: Clarendon Press, 1950.
[16] K. Wulfsberg, private communication.
[17] E. K. Smith and S. Weintraub, "The constants in the equation for atmospheric refractive index at radio frequencies," *Proc. IRE*, vol. 41, pp. 1035–1037, August 1953.
[18] J. H. Davis and J. R. Cogdell, "Astronomical refraction at millimeter wavelengths," *IEEE Trans. Antennas Propagat.*, vol. AP-18, pp. 490–493, July 1970.
[19] T. Oguchi, "Attenuation of electromagnetic wave due to rain with distorted raindrops (pt. II)," *J. Radio Res. Lab. Jap.*, vol. 11, pp. 19–44, 1964.
[20] H. C. Van de Hulst, *Light Scattering by Small Particles*. New York: Wiley, 1957.
[21] J. R. Gerhardt, C. W. Tolbert, S. A. Brunstein, and W. W. Bahn, "Experimental determinations of the backscattering cross sections of water drops and of wet and dry ice spheres at 3.2 centimeters," *J. Meteorol.*, vol. 18, pp. 340–347, 1961.
[22] R. K. Crane, "Microwave scattering parameters for New England rain," M. I. T. Lincoln Lab., Lexington, Mass., Tech. Rep. 426, ASTIA Doc. AD-647798, October 1966.
[23] J. O. Laws and D. A. Parsons, "The relation of raindrop-size to intensity," *Am. Geophys. Union Trans.*, vol. 24, pp. 452–460, 1943.
[24] H. K. Weickmann and H. J. aufm Kampe, "Physical properties of cumulus clouds," *J. Meteorol.*, vol. 10, pp. 204–221, 1953.
[25] E. A. Mueller and A. L. Sims, "Raindrop distributions at Franklin, North Carolina," Illinois State Water Survey Urbana, Ill., Tech. Rep. TR-ECOM-02071-RR3, September 1967.
[26] E. A. Mueller and A. L. Sims, "Relationships between reflectivity, attenuation, and rainfall rate derived from drop-size spectra," Illinois State Water Survey, Urbana, Ill., Tech. Rep. TR-ECOM-02071-F, May 1969.
[27] R. K. Crane, "Simultaneous radar and radiometer measurements of rain shower structure," M. I. T. Lincoln Lab., Lexington, Mass., Tech. Note 1968-33, ASTIA Doc. AD-678079, September 1968.
[28] J. S. Marshall and W. McK. Palmer, "The distribution of raindrops with size," *J. Meteorol.*, vol. 5, pp. 165–166, 1948.
[29] D. M. A. Jones and L. A. Dean, "A raindrop camera," Illinois State Water Survey Res. Rep. 3, Urbana, Ill., December 1953.
[30] J. Joss and A. Waldvogel, "Ein Spectrograph für Niederschlagstropfen mit automatischer Auswertung," *Pure Appl. Geophys.*, vol. 68, pp. 240–246, 1967.
[31] J. W. Ryde and D. Ryde, "Attenuation of centimeter waves by rain, hail, and clouds," General Electric Co., Res. Labs., Wembley, England, Rep. 8516, August 1944.
[32] D. E. Kerr, *Propagation of Short Radio Waves*, Rad. Lab. Series, vol. 13. New York: McGraw-Hill, 1951.
[33] L. J. Anderson, J. P. Day, C. H. Freres, and A. P. D. Stokes, "Attenuation of 1.25-centimeter radiation through rain," *Proc. IRE*, vol. 35, pp. 351–354, 1947.
[34] R. G. Medhurst, "Rainfall attenuation of centimeter waves: comparison of theory and measurement," *IEEE Trans. Antennas Propagat.*, vol. AP-13, pp. 550–564, July 1965.
[35] J. Bell, "Propagation measurements at 3.6 and 11 Gc/s over a line-of-sight radio path," *Proc. Inst. Elec. Eng.*, vol. 114, pp. 545–549, 1967.
[36] B. C. Blevis, R. M. Dohoo, and K. S. McCormick, "Measurements of rainfall attenuation at 8 and 15 GHz," *IEEE Trans. Antennas Propagat.*, vol. AP-15, pp. 394–403, May 1967.
[37] B. J. Easterbrook and D. Turner, "Prediction of attenuation by rainfall in the 10.7–11.7 GHz communication band," *Proc. Inst. Elec. Eng.*, vol. 114, pp. 557–565, 1967.
[38] T. W. Harrold, "Attenuation of 8.6 mm-wavelength radiation in rain," *Proc. Inst. Elec. Eng.*, vol. 114, pp. 201–203, 1967.
[39] J. A. Lane, A. C. Gordon-Smith, and A. M. Zavody, "Absorption and scintillation effects at 3-mm wavelength on a short line-of-sight radio link," *Electron. Lett.*, vol. 3, pp. 185–186, 1967.
[40] G. E. Weibel and H. O. Dressel, "Propagation studies in millimeter-wave link systems," *Proc. IEEE*, vol. 55, pp. 497–513, April 1967.
[41] D. C. Hogg, "Statistics on attenuation of microwaves by intense rain," *Bell Syst. Tech. J.*, vol. 48, pp. 2949–2962, 1969.
[42] R. A. Semplak and R. H. Turrin, "Some measurements of attenuation by rainfall at 18.5 GHz," *Bell System Tech. J.*, vol. 48, pp. 1767–1787, 1969.
[43] S. L. Godard, "Propagation of centimeter and millimeter wavelengths through precipitation," *IEEE Trans. Antennas Propagat.*, vol. AP-18, pp. 530–534, July 1970.
[44] L. J. Ippolito, "Millimeter wave propagation measurements from the Applications Technology Satellite (ATS-V)," *IEEE Trans. Antennas Propagat.*, vol. AP-18, pp. 535–552, July 1970.
[45] J. F. Roche, H. Lake, D. T. Worthington, C. K. H. Tsao, and J. T. deBettencourt, "Radio propagation 27–40 GHz," *IEEE Trans. Antennas Propagat.*, vol. AP-18, pp. 452–462, July 1970.
[46] O. Ya. Usikov, V. L. German, and I. Kh. Vakser, "Investigation of the absorption and scatter of millimeter waves in precipitation," *Ukr. Fiz. Zh.*, vol. 6, pp. 618–641, 1961.
[47] E. A. Mueller, "Raindrop distributions at Miami, Florida," Illinois State Water Survey, Urbana, Ill., Res. Rep. 9b, June 1962.
[48] P. M. Austin, "Frequency of occurrence of rain attenuation of 10 dB or greater at 10 Gc," M. I. T. Weather Radar Res., Cambridge, Mass., December 1966.
[49] J. D. Sartor and W. R. Atkinson, "Change transfer between raindrops," *Science*, vol. 157, pp. 1267–1269, 1967.
[50] R. K. Crane, "Coherent pulse transmission through rain," *IEEE Trans. Antennas Propagat.*, vol. AP-15, pp. 252–256, March 1967.
[51] A. S. Dennis, "Forward scatter from precipitation as an interference source at stations monitoring satellites," Stanford Research Institute, SRI Project 3773, Res. Memo 2 (revised), November 1961.
[52] R. K. Crane, "Predictions of transhorizon field strength using modeling techniques," M. I. T. Lincoln Lab., Lexington, Mass., Tech. Note 1969-53, ASTIA Doc. AD-698335, October 1969.
[53] R. W. Wilson, "Sun tracker measurements of attenuation by rain at 16 and 30 GHz," *Bell Syst. Tech. J.*, vol. 48, pp. 1383–1404, 1969.
[54] R. A. Semplak, "The influence of heavy rainfall on attenuation at 18.5 and 30.9 GHz," *IEEE Trans. Antennas Propagat.*, vol. AP-18, pp. 507–511, July 1970.
[55] R. K. Crane, "Microwave propagation through a turbulent atmosphere," Ph.D. dissertation, Dept. of Elec. Engrg., Worcester Polytechnic Institute, Worcester, Mass., December 1969.
[56] V. I. Tatarski, *Wave Propagation in a Turbulent Medium*. New York: McGraw-Hill, 1961.
[57] J. A. Lane, "Scintillation and absorption fading on line-of-sight links at 35 and 100 GHz," presented at Tropospheric Wave Propagation IEE Conference, Pub. no. 48, 1968.
[58] H. B. Janes, M. C. Thompson, Jr., D. Smith, and A. W. Kirkpatrick, "Comparison of simultaneous line-of-sight signals at 9.6 and 34.5 GHz," *IEEE Trans. Antennas Propagat.*, vol. AP-18, pp. 447–451, July 1970.
[59] R. W. Lee and A. T. Waterman, "Space correlation of 35 GHz transmissions over a 28 km path," *Radio Sci.*, vol. 3, pp. 135–140, 1968.
[60] R. K. Crane, "Monostatic and bistatic scattering from thin turbulent layers in the atmosphere," M. I. T. Lincoln Labs., Lexington, Mass., Tech. Note 1968-34, September 1968.

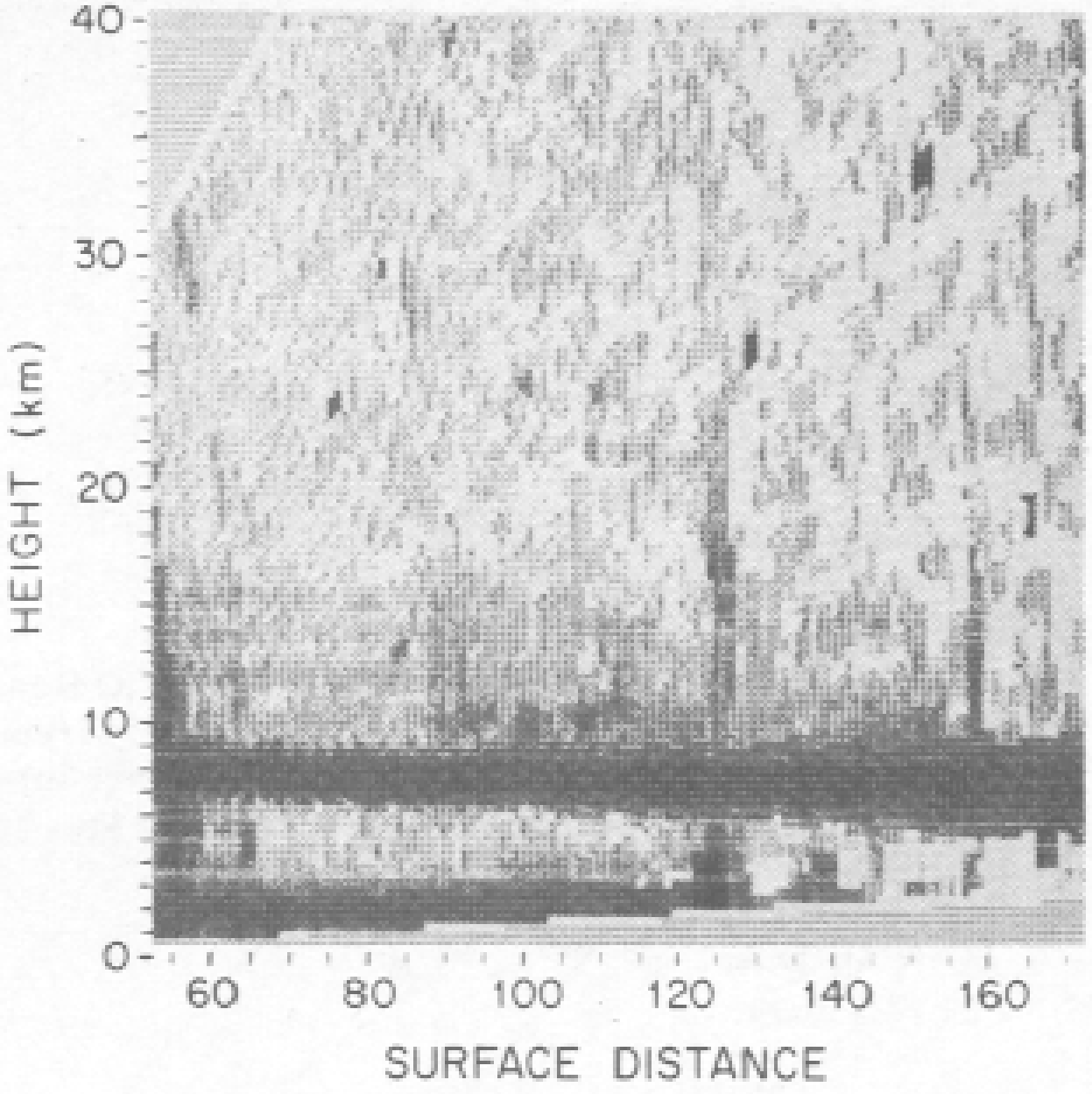

Fig. 21. RHI display. Millstone Hill *L*-band radar.